Using CASI Hyperspectral Imagery to Detect Mortality and Vegetation Stress Associated with a New Hardwood Forest Disease

Ruiliang Pu, Maggi Kelly, Gerald L. Anderson, and Peng Gong

Abstract

A Compact Airborne Spectrographic Imager-2 (CASI) dataset was used for detecting mortality and vegetation stress associated with a new forest disease. We first developed a multilevel classification scheme to improve classification accuracy. Then, the CASI raw data were transformed to reflectance and corrected for topography, and a principal component (PC) transformation of all 48 bands and the visible bands and NIR bands were separately conducted to extract features from the CASI data. Finally, we classified the calibrated and corrected CASI imagery using a maximum likelihood classifier and tested the relative accuracies of classification across the scheme. The multilevel scheme consists of four levels (Levels 0 to 3). Level 0 covered the entire study area, classifying eight classes (oak trees, California bay trees, shrub areas, grasses, dead trees, dry areas, wet areas, and water). At Level 1, the vegetated and non-vegetated areas were separated. The vegetated and non-vegetated areas were further subdivided into four vegetated (oak trees, California bay trees, shrub areas, grasses) and four non-vegetated (dead trees, dry areas, wet areas, and water) classes at Level 2. Level 3 identified stressed and non-stressed oak trees (two classes). The ten classes classified at different levels are defined as final classes in this study. The experimental results indicated that classification accuracy generally increased as the detailed classification level increased. When the CASI topographically corrected reflectance data were processed into ten PCs (five PCs from the visible region and five PCs from NIR bands), the classification accuracy for Level 2 vegetated classes (non-vegetated classes) increased to 80.15 percent (94.10 percent) from 78.07 percent (92.66 percent) at Level 0. The accuracy of separating stressed from non-stressed oak trees at Level 3 was 75.55 percent. When classified as a part of Level 0, the stressed and non-stressed were almost inseparable. Furthermore, we found that PCs derived from visible and NIR bands separately yielded more accurate results than the PCs from all 48 CASI bands.

Ruiliang Pu is with the Department of Geography, University of South Florida, 4202 East Fowler Ave., NES 107, Tampa, FL 33620 (rpu@cas.usf.edu).

Maggi Kelly and Peng Gong are with the Center for Assessment & Monitoring of Forest & Environmental Resources (CAMFER), 137 Mulford Hall, University of California, Berkeley, CA 94720.

Gerald. L. Anderson is with the USDA, Agricultural Research Service, 1500 N. Central Ave., Sidney, MT 59270.

Introduction

A new canker disease called sudden oak death (SOD) (Rizzo and Garbelotto, 2003) is affecting tree and shrub species, including coast live oak (*Quercus agrifolia*), tanoak (*Lithocarpus densiflorus*), and black oak (*Q. kelloggii*) along 300 km of the central California coast. The disease, caused by a newly discovered virulent pathogen called *Phytophthora ramorum* is reaching epidemic proportions in the region. The pathogen is lethal for many individual trees of these species. On susceptible trees, the pathogen can enter the bark and kill phloem tissue restricting translocation of water and nutrients in the tree. It can take two or more years for a tree to die (McPherson *et al*., 2005). However, once crown dieback begins, the foliage of infected trees appears to die rapidly with leaves changing color from dark green to pale yellow and brown in just a few weeks (McPherson *et al*., 2000; Garbelotto *et al*., 2001). SOD has attracted substantial public attention because oaks are major components of California hardwood forest ecosystems, urban areas, and the urban/rural interface (Rizzo and Garbelotto, 2003). Early detection of the disease would improve the ability of managers to deal with disease outbreaks. One possible method of early detection and assessment is remote sensing.

Remote sensing of vegetation relies on a thorough understanding of the biophysical and biochemical characteristics of plants and their canopies. Parameters such as crown closure, leaf area index, canopy structure, chlorophyll content, foliar nutrients, and foliar water content are all important indicators of vegetation health (Curran, 1989; Elvidge, 1990; Cibula *et al*., 1992; Belanger *et al*., 1995; Hall *et al*., 1998; Ceccato *et al*., 2001; Gerylo *et al*., 2002; Gong *et al*., 2003; Pu *et al*., 2003a and 2003b). Previous research was used to evaluate the utility of multispectral sensor data for mapping tree mortality in forest areas affected by disease or stress. Kelly and Meentemeyer (2002) and Kelly *et al*. (2004) used high-resolution Airborne Data Acquisition and Registration Imagery (ADAR) imagery to map dead and dying oak trees in Marin County, California. Similarly, Everitt *et al*. (1999) reported that oak wilt disease could be detected using airborne digital imagery in south-central Texas, while Macomber and Woodcock (1994) used Thematic Mapper (TM) imagery to map conifer mortality resulting from drought. Their study

Photogrammetric Engineering & Remote Sensing
Vol. 74, No. 1, January 2008, pp. 65–75.

0099-1112/08/7401–0065/$3.00/0

examined the utility of broad-band remote sensing data in forest hazard management by providing both locations and estimates of dead trees. All of the aforementioned authors found that they could distinguish dead crowns from the healthy forest mosaic using digital multispectral imagery. Kelly and Liu (2004), on the other hand, found it difficult to distinguish different health levels of diseased trees using multispectral data (ADAR).

Hyperspectral remote sensing has proven useful for mapping vegetation and detecting vegetation stress at both the leaf and canopy scales. Hyperspectral data products have been particularly useful for extracting biochemical parameters like chlorophyll and tree leaf moisture content. For example, Peñuelas *et al*. (1993 and 1996) used reflectance measured in the 950 to 970 nm region to detect gerbera, pepper, bean, and wheat plant water status. Their results demonstrated that the ratio of reflectance at 970 nm to the reflectance at 900 nm could be used to closely track changes in relative water content (RWC), leaf water potential, stomatal conductance and cell wall elasticity. Tian *et al*. (2001) evaluated the spectral absorption features (between 1650 and 1850 nm) and RWC of wheat leaves to study the feasibility of diagnosing wheat-water status. Their findings indicated a correlation between spectral absorption features (depth, area, and wavelength position) and RWC of wheat leaf samples. Imanishi *et al*. (2004) conducted a field experiment using three-year-old potted *Quercus glauca* and *Q. serrata* to examine the utility of derivative spectrum analysis for detecting drought status and LAI at canopy level and to find the optimal bands that can independently detect those variables. The best single bands for detecting leaf water content and LAI were 519.6 nm in the first derivative ($r = 0.916$) and 676.0 nm in the second derivative ($r = 0.828$), respectively. By extracting spectral features from lab-measured hyperspectral data, Pu *et al*. (2003b and 2004) showed that RWC of oak leaves was correlated with spectral absorption features across the spectrum, particularly at 975 nm, 1,200 nm, and 1,750 nm, and the hyperspectral data has also proved useful in measuring vegetation stress (Pu *et al*., 2004). Stressed leaves show a stark difference in their major pigment concentrations and water content as compared to non-stressed leaves. This indicates that the narrow spectral resolution of hyperspectral data is sensitive enough to discern spectral differences between stressed and non-stressed leaves, differences that broad spectral band sensor data cannot.

As a complement to such a lab-measured spectral analysis, hyperspectral imagery has been useful in measuring biophysical and biochemical parameters at broad scales. Curran *et al*. (1997) used the Airborne Visible/Infrared Imaging Spectrometer (AVIRIS) hyperspectral system to analyze the water content of slash pine needles. Results indicated an R^2 of 0.99 for pine needle water status when three absorption bands (975 nm, 1,200 nm, and 1,750 nm) were used in a five-term multivariate regression model. At the canopy scale, Ustin *et al*. (1998) found that moderate resolution (20 m) AVIRIS data could potentially be used on a regional scale to estimate the water content of chaparral shrub canopies. Johnson *et al*. (1994) determined predictive relationships for biochemical concentrations using regressions between the chemical composition of forest canopy and AVIRIS reflectances. Using data from AVIRIS and a Compact Airborne Spectrographic Imager (CASI), Matson *et al*. (1994) demonstrated that canopy biochemicals carried information about forest ecosystem processes and suggested that some of this chemical information might be estimated remotely using hyperspectral data collected by airborne sensors. Wessman *et al*. (1988 and 1989) reported a significant correlation between mid-infrared radiance data from Airborne Imaging Spectrometer (AIS) and canopy lignin, and nitrogen availability in both deciduous and coniferous stands. In addition, some physically based models (e.g., radiative transfer models) have been successfully used to simulate leaf reflectance and transmittance and to estimate leaf biochemical properties. For example, Haboudane *et al*. (2002) employed PROSPECT and SAILH radiative transfer models to retrieve leaf chlorophyll content from hyperspectral CASI imagery collected over corn crops in three experimental farms from Ontario and Quebec, Canada by simulating leaf and canopy reflectance with the models. Evaluation showed chlorophyll variability over crop plots with various levels of nitrogen, and revealed an excellent agreement with ground truth. Sampson *et al*. (2003) developed an inverse modeling approach that demonstrated that the CASI could be used to map chlorophyll content following different silvicultural treatments in a tolerant hardwood (sugar maple (*Acer saccharum M.*)) forest. This capability could be readily applied to operationally assessing forest physiological strain and in classifying forest condition based on chlorophyll content at a canopy level. Recently, Hyperion hyperspectral data were used to predict and estimate forest nitrogen (Smith *et al*., 2003; Coops *et al*., 2003; Townsend *et al*., 2003).

Based on the previous work and initial examination of SOD by Pu *et al*. (2003b and 2004), we suspected that the foliage of infected trees, even when they appear green, have a different water and biochemical status as compared to healthy leaves. If, in addition to mapping hardwood mortality, we could detect SOD infected oak trees at a much earlier stage (before the leaves have undergone dramatic shifts in pigmentation), we could give managers a significant advantage in dealing with the disease. This led us to examine mortality and vegetation stress using hyperspectral data from CASI in China Camp State Park, Marin County, California. We know from previous work that the spectral difference between healthy and stressed oak leaves sampled from the Marin County study site is very slight (Pu *et al*., 2004). In that work the maximum (or minimum) 1st derivative (1D) and its corresponding wavelength position (WP) were extracted from ten spectral slopes along each spectral reflectance curve of a total of 306 coast live oak leaf samples to test the relationships between the 20 spectral features and RWC (percent). We also tested the spectral difference between two health levels of oak leaves, healthy and infected. The result of an analysis of variance (ANOVA, SAS Institute, Inc., 1991) of 20 spectral features suggests that the difference of a few of spectral features between two health levels of oak leaves is significant at a 0.95 confidence level, but there exists a relatively large variation within individual health levels (Pu *et al*., 2004). Given this slight difference, we predicted that the stressed trees would be almost inseparable from other trees if we were to use a standard classification strategy. Therefore, we developed a multilevel classification system (Townsend and Walsh, 2001) to detect SOD with CASI imagery. The multilevel classification scheme described in this paper represents a flexible approach to vegetation mapping and general classification that can be applied to detect or monitor hardwood mortality and crown dieback. Additionally, the flexibility of the scheme provides the potential for increased detail and accuracy in the final classification and permits the expansion and refinement without revising the entire classification (Richards, 1993). Our experimental objectives in this study include: (a) evaluating the performance of the multilevel classification scheme, (b) comparing the effectiveness of two data preprocessing approaches of calibrating and topographically correcting the CASI data, and (c) assessing the effect on the classification accuracy of two feature extraction methods over ten features each.

Study Site and Analysis Data

Study Site

China Camp State Park was chosen as our study site (Plate 1). The park is located in a forested peninsula on the east side of Marin County, California (122°29′50″W, 38°00′30″N). The topography of the area is composed of moderate to steep slopes (10° to 40°) with elevations ranging from sea level to over 300 m. The major forest types include coast live oak, black oak, and valley oak (*Q. lobata*) occurring in mixed stands with mature madrone (*Arbutus menziesii*) and California bay trees (*Umbellularia californic*, all of which, with the exception of the valley oak, are hosts for *P. ramorum* (Rizzo *et al.*, 2002)). The forest stand we examined is of even-age trees with a largely continuous canopy. Individual trees have moderately large crowns that range from 4 m^2 to 16 m^2. Sudden oak death was first reported in the area in 1997, and the disease became widespread here through 2004 (McPherson *et al.*, 2000; Kelly, 2002).

CASI Imagery

CASI has been in commercial production since 1989. It is a charge couple device (CCD) pushbroom imaging spectrograph intended for the acquisition of visible and near-infrared hyperspectral imagery. CASI offers a multispectral mode (programmable bands) and a hyperspectral data cube mode. CASI operates over a 545 nm spectral range between 400 nm and 1000 nm and has a cross-track field of view of 37.8°. The spectral and spatial resolution of the instrument can be changed from sub-meter to 10-meter pixels, and the hyperspectral mode can collect up to 288 bands. Operationally, the user can trade spatial resolution for spectral resolution, thus optimizing the quantity of data collected.

In this study, the United States Department of Agriculture, Agricultural Research Service, Sidney, Montana collected the CASI imagery with 48 spectral bands of approximately 11 nm on 02 July 2002. The 48 bands were systematically (equal interval) selected from a total of 288 bands, i.e., picking one every six bands. The original spatial resolution of the CASI

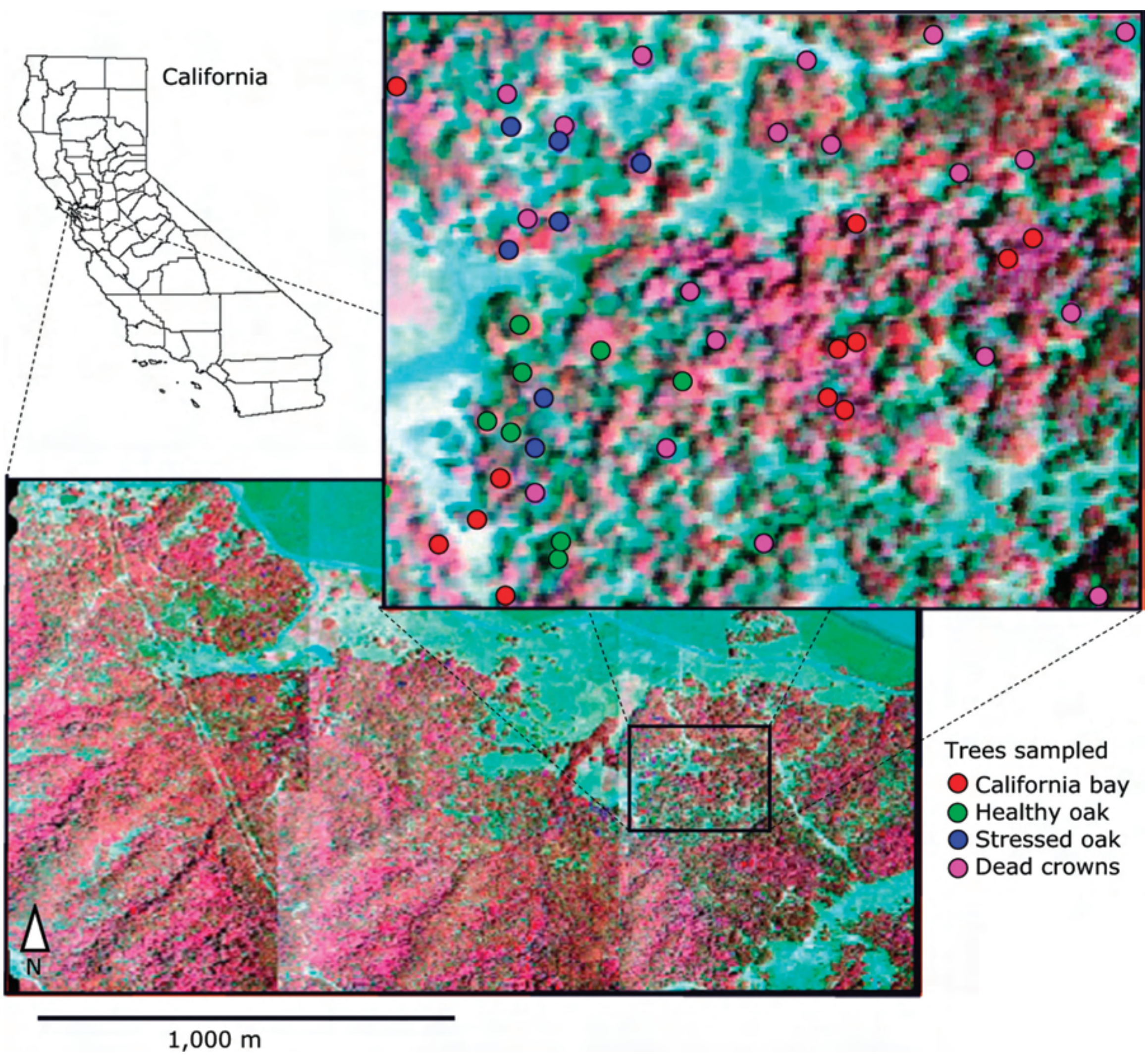

Plate 1. The location of study area and partial training and test areas on a false color CASI image. The green color dots locate healthy trees; the blue ones locate stressed trees; the pink ones are dead trees; and the red ones are California bay trees.

data was 2 m. The 2 m data was simply resampled to 1 m to fit other higher spatial resolution data. We performed topographic correction on the CASI imagery using a digital elevation model (DEM) at 5 m spatial resolution. The DEM model was previously derived from photogrammetric methods using black and white stereo aerial imagery.

ASD Full Range Hyperspectral Radiometer

Ground spectral data collected from light and dark targets located in the CASI scenes were acquired using a full-range Analytical Spectral Device (ASD) (FieldSpec®ProFR). The ASD data, collected on 23 July 2002, were used to calibrate the raw CASI data from radiance to reflectance. The targets included a white target, a parking lot, dry grasses, dense shrubs, a water-ditch, an asphalt-road surface, and a dense coast live oak canopy. The ASD instrument consists of three separate spectrometers and covers a spectral range of 350 nm to 2,500 nm. The first spectrometer has a spectral resolution of 3 nm, and the second and third have a spectral resolution of approximately 10 nm. Calibration of the CASI data was accomplished using data from the first spectrometer. All spectra were measured at nadir with a 25° field of view. The distance between the spectrometer and the targets ranged from 50 cm to 100 cm, depending on target characteristics. Ten separate measurements were acquired from each target.

ADAR Imagery

In addition to the CASI data and ground spectral measurements, ADAR 5500 data were collected in spring 2002 and in summer 2003. The ADAR 5500 is airborne multispectral sensor and has four spectral bands: band 1 (blue, 450 to 550 nm), band 2 (green, 520 to 610 nm), band 3 (red, 610 to 700 nm), and band 4 (near infrared, 780 to 920 nm). These data were used with field data to extract samples of healthy, stressed, and dead oak trees. The aircraft with the ADAR sensor was flown at an average altitude of 2,205 m, with an average ground resolution of 1 m (for more details see Kelly *et al.*, 2004).

Methodology

A Multilevel Classification Scheme

We developed a multilevel classification scheme (Figure 1) for the project. One advantage of this methodology is that it matches the logical structure of most plot-based floristic classification schemes (Townsend and Walsh, 2001). The multilevel classification scheme was constructed in four levels (Figure 1). Level 0 is for the entire study area, and the classification of all eight classes (oak trees, California bay trees, shrub areas, grasses, dead trees, dry areas, wet areas, and water) is conducted at this level. At this level, a traditional classification result would be produced in order to be compared with results generated at higher levels. At Level 1, two sub-areas, vegetated and non-vegetated, are separated using an NDVI threshold of 0.3. NDVI values greater than 0.3 were assigned as vegetation. With this threshold, the two sub-areas could be clearly separated within the study area. The vegetated and non-vegetated areas were further subdivided into four vegetated and four non-vegetated classes at Level 2 using a maximum likelihood classifier (MLC). The four vegetated types include oak trees (coast live, black, and valley oaks), California bay trees, shrubs, and living grasses including meadow. The four non-vegetated classes include dead trees, dry areas (consisting of dry bare soil, concrete/asphalt, and dry grasses), wet areas (wet bare soil, wet dead grasses), and water. The finest level of detail, Level 3, is further subdivided the oak tree class into two classes, stressed and non-stressed (for their

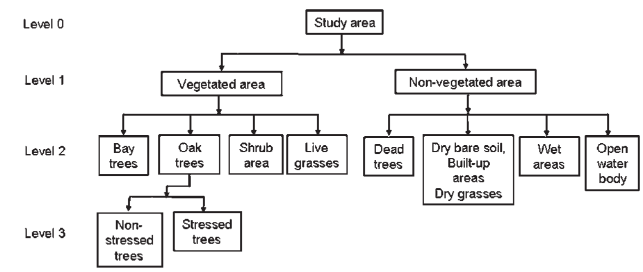

Figure 1. A multilevel classification scheme: Level 0 with the entire study area; Level 1 with NDVI >0.3 as vegetated area, otherwise as non-vegetated area; Level 2 with two 4-vegetated classes (Bay trees, Oak trees, Shrub area and Live grasses) and four non-vegetated classes (Dead trees, Dry areas, Wet area, and Water body), Level 3 with two oak health levels: healthy and stressed. A traditional maximum likelihood classifier (MLC) was applied to classification at Levels 0, 2, and 3.

identification, see the section "Extraction of Training and Test Samples"). Therefore, the two oak health classes (Level 3) only relate to oak tree classes that were classified from the four vegetated classes (Level 2) which are components of the vegetated sub-area (Level 1). The purpose of further classification of the four non-vegetated classes was to detect the dead trees (oak mortality).

Data Preprocessing Approaches

In this study, two data preprocessing approaches were applied: first, calibration of CASI radiance data into reflectance values and second, topographic correction to the reflectance values. Calibration of CASI data was accomplished using a well-known empirical band-to-band linear regression model (Freemantle *et al.*, 1992; Goetz *et al.*, 1997):

$$\mathbf{Y} = \mathbf{AX} + \mathbf{B} \tag{1}$$

where **Y** denotes a spectral vector taken from a ground target with the ASD spectrometer, **X** represents CASI pixel spectral vector digital number (DN) values; **A** and **B** are slope and intercept vectors of the **X, Y** regression line, respectively. The **B** intercept vector is described as an offset of radiance for each band induced by atmospheric path radiance, while the **A** slope vector accounts for atmospheric transmittance differences and spectral shifts caused by the instrument. The CASI reflectance image was then topographically corrected using the following approach.

Topographic normalization of imagery removes the influence of slope and aspect from the observed spectral reflectance or radiance values (Allen, 2000). An ideal slope-aspect correction model removes all topographically induced illumination variation. Therefore, objects having the same reflectance properties have similar DN despite their orientation to the sun's position (Meyer *et al.*, 1993). The procedure used for correction was based on previous work by Townsend and Foster (2002), Allen (2000), and Meyer *et al.* (1993). We assumed that a linear relationship existed between illumination and spectral reflectance (radiance). This relationship was used to remove the confounding effects of topography. The linear regression model takes the form:

$$L_H = L_T - \cos(i)m - b + \bar{L}_T \tag{2}$$

where, L_H is radiance observed for horizontal surface, L_T is radiance observed over slope terrain, $\bar{L}_T$ is average radiance of L_T for forest pixels or other specific cover types in a scene of image, i is sun incidence angle in relation to the normal of a pixel, and m and b are the slope and intercept of the regression line, respectively. The pixel-based sun incidence angle values can be derived using PCI Geomatica® software (PCI Geomatics, Ontario, Canada) using a DEM model and the sun position in association with the date and time when the image was acquired. It is worth noting that the effectiveness of topographic correction depends on what cover type in the scene is used for deriving parameters in Equation 2. In this study, since we emphasize on mapping mortality and detecting oak tree stress associated with a new disease (SOD), all the parameters in Equation 2 were derived from the oak tree class in the study area.

Feature Extraction Methods

Feature selection is one challenge inherent in using hyperspectral data. With tens and sometimes hundreds of bands from which to choose, the analyst must determine which bands or features to include in a classification scheme. In hyperspectral remote sensing, it is well known that classification with all spectral bands can lead to lower accuracies (Gong *et al.*, 1997; Hsu *et al.*, 2002). This is due to cross correlation issues across classes (Yu *et al.*, 1999). We chose principal component analysis (PCA) to extract features from CASI hyperspectral data and evaluated the PCs for their utility in discriminating classes at different classification levels. PCA along with Kauth-Thomas transformation (KT) (a specialized Gramm-Schmidt orthogonalization) has been broadly applied in change detection (e.g., Gong, 1993; Collins and Woodcock, 1996; Hayer and Sader, 2001).

Method 1 Five Principal Components from the Visible Bands and Five from the NIR Bands

Principal component analysis was performed on 25 bands in the visible region of the CASI data (420 to 705 nm) and on 23 bands in the near infrared (NIR) region (705 to 970 nm) separately. A total of ten principal components (PC) were extracted, five of which were from visible bands and five of which were from NIR bands. Separate extraction of PCs from visible and NIR regions was done to maximize available information obtained from the lower variability data of the visible region relative to that from the NIR region, which typically has higher variability in its data.

Method 2 First Ten Principal Components

The first ten PCs were extracted from the entire 48-band CASI data cube without regard for differences in variability in the visible or NIR regions.

Classification Algorithm

A traditional MLC was applied to four datasets (two data preprocessing approaches by two feature extraction methods) in order to detect mortality and vegetation stress associated with the disease. Determining the accuracy of the classification results was accomplished using average accuracy (AA) assessment, overall average accuracy assessment (OAA), and the Kappa-Variance (K-V) as accuracy and statistical indices (Congalton and Mead, 1983; Fung and LeDrew, 1988). All those accuracy indices were calculated from independent test samples. The K-V was used to calculate a Z-statistic ($Z = \frac{|k_1 - k_2|}{\sqrt{v_1 + v_2}}$, where, k_1 and k_2 are kappa values of corresponding Method 1 and Method 2, respectively, and v_1 and v_2 are corresponding variances) that was used to test the difference in accuracy between data preprocessing approaches and between feature extraction methods.

Extraction of Training and Test Samples

Field surveys and comparison of multitemporal ADAR imagery were used to extract four different training and test samples from the CASI datasets. The eight cover types (the first eight classes in Table 1) were also outlined on a hardcopy of the CASI image. In order to separate the two oak health levels (stressed and non-stressed), we examined previously-acquired ADAR imagery from 2003 and 2002. The locations of 118 healthy coastal live oak trees with medium to large crowns (>3 m diameter), green foliage, and no SOD symptoms on the tree trunk were located either using GPS or by comparing the differences between the 2002 and 2003 ADAR imageries. The locations of 81 stressed coast live oak trees with medium to large green crowns were found by first finding individual trees in the 2003 ADAR imagery that already were dead but appeared healthy in the 2002 ADAR imagery. We then located 40 individuals from the 81 stressed oak trees in the field with GPS and made a note on the hardcopies of the 2002 CASI and ADAR imagery, which helped confirm the remaining stressed oak trees identified in the ADAR imagery. Stressed trees had advanced symptoms on the main stem (extensive cankering and bleeding) and were within one year of changing color from green to brown. Plate 1 presents examples of Bay, healthy oak, stressed oak, and dead trees.

After delineating training and test areas of all ten classes on the CASI imagery, we extracted their pixel spectra. Table 1 lists numbers of pixel samples of all ten classes. The sample sizes (Table 1) are significantly different among the ten classes, which is because selection of sample size was difficult for some classes, such as two health levels of oak trees and shrub class, due to limited numbers of oak trees (reliably separating stressed and non-stressed) and shrub class (identified). According to the individual crown size, 10 to 50 pixel samples were extracted from the CASI imagery for one individual tree.

Results

Data Preprocessing

Since both CASI and ASD data were acquired near noon under a clear sky condition, the influence on both datasets by the atmospheric and BRDF effects were relatively weak. A simple linear model Equation 1 was therefore applicable and was used to calibrate the CASI radiance to reflectance. Consequently, the six targets (a parking lot, dry grasses, dense shrubs, a water-ditch, an asphalt-road surface, and a dense coast live oak canopy) were selected from the CASI imagery and in the field with two requirements: relative homogeneity within individual target areas, and patch sizes no smaller than 9 (3 × 3) CASI pixels (36 m^2). The six

TABLE 1. PIXEL SAMPLES EXTRACTED FROM CASI IMAGERY USED IN THIS ANALYSIS

Class Name	Training Samples	Test Samples	Total
Bay trees	3664	3884	7548
Oak trees	6137	7157	13294
Shrub	996	965	1961
Grasses	3832	3582	7414
Dead trees	4519	4297	8816
Dry areas	12976	12357	25333
Wet areas	10335	12230	22565
Water	5902	8294	14196
Non-stressed oaks	2188	1819	4007
Stressed oaks	1808	1909	3717
	52357	**56494**	**108851**

targets were selected because they represent nearly the whole range of spectral variation in the study area (from bright to dark targets). CASI DN curves were extracted from six targets, averaged by 4 to 9 CASI pixels, and the plot of six ASD curves each was averaged by ten measurements. These are shown in Figure 2a and 2b. Figure 2c shows the R^2 between CASI DN and ASD reflectance data for each band. The R^2 values for individual bands were calculated from six samples (i.e., the six curves in Figure 2a and 2b). Comparative observation indicated that the CASI DN curves are subject to a significant variation, particularly in the NIR region (Figure 2a). This supposition is supported by the ASD spectrometer data, which are much smoother (with less variation) in this region (Figure 2b). Figure 2c shows the R^2 between CASI DN and ASD reflectance data for each band. The R^2 values of all bands (except for the 700 nm band) are either close to or greater than 0.9, indicating a reliable functional relationship between the two devices in most regions of the electromagnetic spectrum. The ASD data, therefore, can be used to calibrate the CASI DN to reflectance values. Some of the differences found between ASD and CASI spectra might be due to the different full-width-half-maximum (FWHM) of both instruments (3 nm and 11 nm), especially at 700 nm, a region or rapid reflectance increase (the so-called "red edge" reflectance range) due to leaf pigment absorption and leaf structure scattering. Figure 2d presents the six CASI reflectance curves after conversion to reflectance. The converted reflectance curves shown in Figure 2d are very similar to original ASD reflectance curves shown in Figure 2b, with the exception of the band near 700 nm. The cause of the low R^2 value at that point (Figure 2c) was undetermined.

Equation 2 was used to correct all slope-aspect pixel values (reflectance) to horizontal pixel values based on sun orientation. Figure 3a and 3b present the results of the terrain normalization of CASI converted reflectance imagery with Equation 2 whose parameters were simulated from the pixel samples of the oak tree class in the study area. The topographic normalization, in large part, corrected for the influence of terrain on CASI reflectance pixel values. It also de-trended pixel values dependant on the slope and aspect of the terrain. The effects of this normalization are especially apparent when comparing the corrected and uncorrected data.

Multi-level Classification

The multi-level classification scheme was used to increase the classification accuracy of end-classes. Table 2 lists the producer and user classification accuracies as well as the average and overall accuracies of the different classification levels. Differences in classification accuracies for Level 2 and Level 0 (the four vegetated classes and four non-vegetated classes) are significantly different (alpha = 0.01) with accuracies increasing as levels increase (average accuracies). Due to their similar spectral characteristics, the Level 0 (eight-class) scheme could not differentiate between stressed and non-stressed oaks. However, the stressed and non-stressed oak trees could be differentiated at Level 3 even when they were

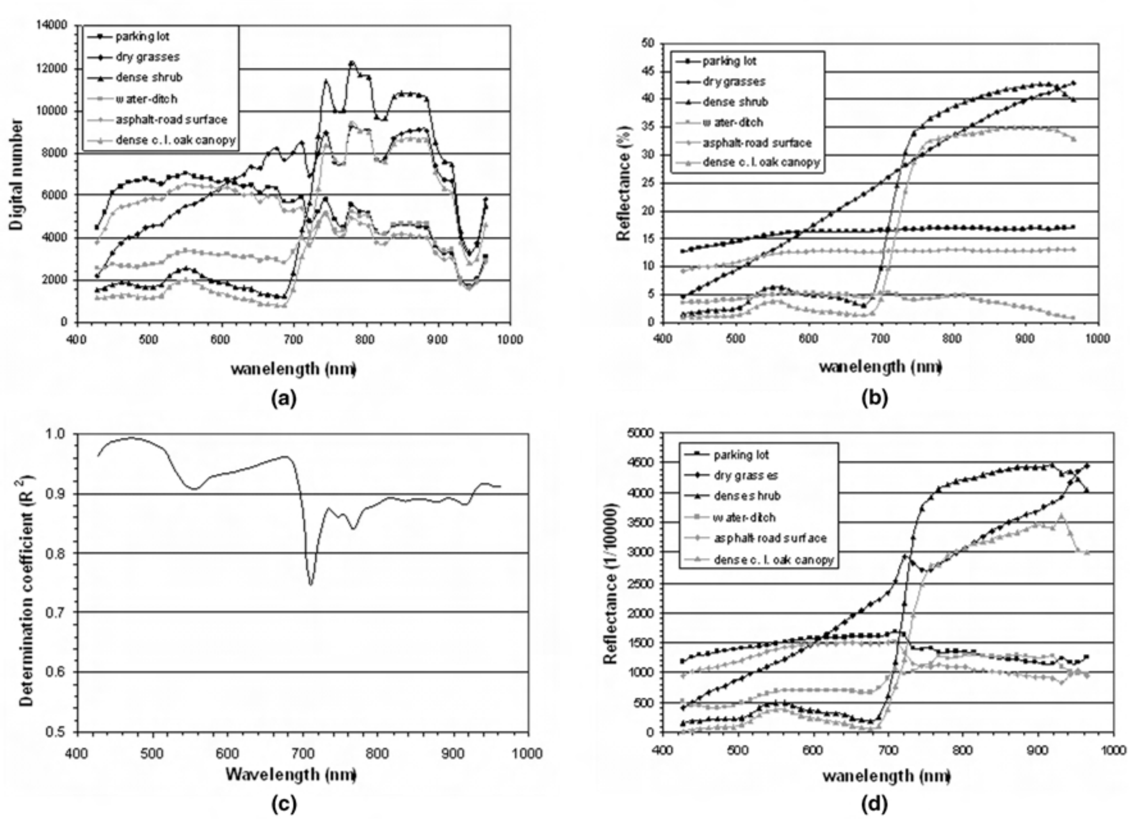

Figure 2. CASI hyperspectral data calibrated from digital (radiance) to reflectance: (a) CASI raw data (digital number), (b) ASD spectral measurements taken from the same targets on the ground as (a), (c) band to band correlation between ASD spectral reflectances and CASI raw data, and (d) CASI converted reflectances.

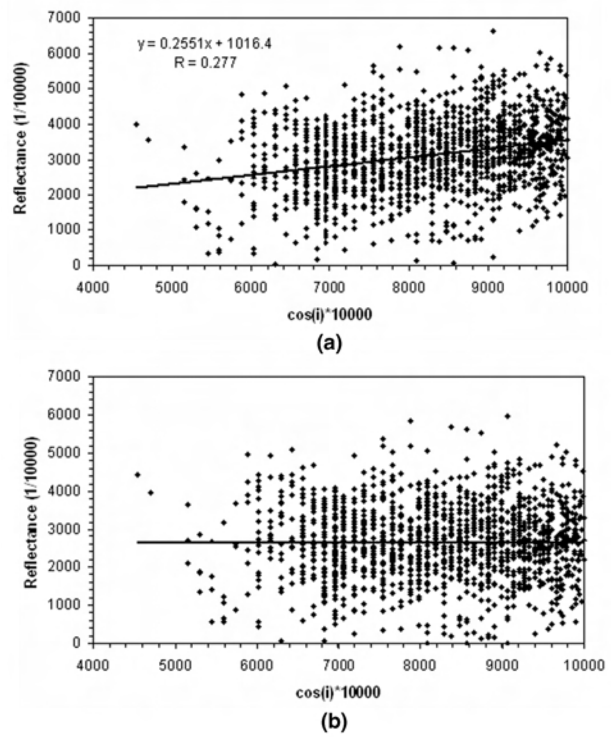

Figure 3. Scatter plots of topographic normalization to CASI data (in converted reflectance): (a) CASI converted reflectance of band 40 versus solar incidence angle (cos(i)*10000), and (b)after topographic normalization to (a).

the only two classes present. To assess the final producer's accuracy in identifying oak health levels, we also considered the classification accuracy of the oak class in the vegetated group at lower levels. For this case, the non-stressed oak trees can be identified with a joint accuracy of 77.20 (Level 2) × 78.20 (Level 3) = 60.37 percent, while the stressed oak trees had a joint accuracy of 77.20 (Level 2) × 72.90 (Level 3) = 56.28 percent (Table 2). While the joint identification accuracy is relatively low, the spectral similarity between the two health levels of oak trees reinforces the observation that the multilevel scheme is able to increase accuracy as a results of an increase in the relative spectral separability with higher classification levels (Levels 2 and 3).

We evaluated the accuracy of each data preprocessing approach and feature extraction method (Table 3). The underlined value represents the greatest accuracy across the two data preprocessing approaches and the two feature extraction methods at one classification level (Table 3). The *Z*-statistics (data not shown) tested for a significant difference between the two classification accuracies with two feature extraction methods and the two data preprocessing approaches. Based on these statistics, the results suggest that the PCs extracted from visible and NIR bands separately were more useful (Table 4) than the PCs from all 48 bands for classification at all levels except for the classification of vegetated classes at Level 2, especially for the identification of the two health levels of oaks at Level 3. The results also imply that topographic correction could favor vegetation classification (Level 2 for four vegetated classes and Level 3 for the identification of two oak health levels). This is because the slope-aspect normalization model (from Equation 2) was simulated under consideration of the oak forest type. In identifying the two oak health levels, we further analyzed the differences in accuracy between the two data preprocessing approaches and two feature extraction methods with *Z*-statistics, listed in Table 4. While focusing on the PCA from visible and NIR bands separately, the OAA calculated with the data preprocessing approaches has a certain difference.

Discussion

In this comparative analysis of classification at four different levels with two data preprocessing types and two feature extraction methods, we found that the classification accuracies are not consistent across classification levels or methods (Table 3). We have two possible technical explanations, as well as some considerations about our particular situation. The first technical consideration is that the response values of the 48 CASI bands, especially the 23 bands located in NIR region, need internal calibration. The second is that the calibration procedure of CASI data using Equation 1 may lower the variance contained in the original data set. This may also directly influence the separability of some cover types. This phenomenon of lowering the variance of the original data set is common, and CASI data calibration followed by a topographic normalization may be more pronounced. For example, the topographically-corrected reflectance preprocessing approach for the eight class scheme in Table 3 resulted in the lowest classification accuracy across the two feature extraction methods and the two data preprocessing approaches. However, converted reflectance data followed by topographic normalization should prove to be very helpful when comparing two data sets acquired at different locations or different times.

Our critical goal was to identify the two health levels of oak trees (Level 3), and we found that the feature extraction method using PCs from visible and NIR bands separately was effective (Table 3). A typical plant spectrum has lower reflectance in the visible region (light is absorbed by various pigments) and a higher reflectance in the NIR region (radiation is scattered by plant cell structure). Compared to the variation of reflectance in NIR, the spectral variation in the visible region is much smaller. However, the visible region contains a larger amount of more stable plant spectral information than the NIR region does, e.g., information of pigment variation, making it more helpful to the classification of the two oak health levels (Gong *et al.*, 1997; van Aardt and Wynne, 2001). When features are extracted by PCA and executed separately to visible bands and NIR bands, maximum spectral information can be preserved in PCs derived from visible and NIR regions. When features are extracted by a PCA executed on all 48 bands, the first several components may account for most variance in the NIR region, thus the valuable information found in the visible region is used inefficiently. This partly explains why the results of the first ten PCs were poorer than those derived with the five PCs extracted from each of the visible and NIR regions for the classification of the two oak health levels.

Although we discriminated between the two oak health levels at a more detailed classification level (Level 3), the greatest OAA was only approximately 75 percent across two feature extraction methods and two data preprocessing approaches used in this analysis (Table 3). Additionally, the greatest accuracy for the non-stressed and stressed oak classes at Levels 2 and 3 were approximately 60 percent and approximately 56 percent, respectively. The accuracy was slightly influenced by shade and shadow. If we consider the full influence of shade and shadow on the final classification result, the final classification accuracy for the two

Table 2. Confusion Matrices at Different Classification Levels Calculated with the Visible and nir Principal Component Feature Extraction Method and the casi Topographically Corrected Reflectance Data

		Reference										Summary	
	Level 0	Bay tree	Oak tree	Shrub	Grass	Dead tree	Dry area	Wet area	Water	Sum	User's %	Average accuracy (%)	**84.53**
	Bay tree	2967	852	49	14	73	12	0	0	3968	74.78	Overall accuracy (%)	**88.08**
	Oak tree	719	5475	140	0	26	0	0	0	6359	86.10	Kappa	**0.85829**
	Shrub	70	687	622	161	241	25	61	0	1867	33.34	Standard Deviation	**0.00166**
Classified	Grass	31	0	88	3274	30	25	183	0	3631	90.16		
	Dead tree	97	136	64	18	3794	494	1541	0	6144	61.75	4 vegetated classes:	
	Dry area	0	7	2	100	77	11665	0	58	11910	97.94	Average accuracy (%)	**78.07**
	Wet area	0	0	0	14	56	0	10444	0	10515	99.33	Overall accuracy (%)	**79.62**
	Water	0	0	0	0	0	136	0	8236	8372	98.38	4 non-vegetated classes:	
	Sum	3884	7157	965	3582	4297	12357	12230	8294	52766	–	Average accuracy (%)	**92.66**
	Producer's %	**76.40**	**76.50**	**64.50**	**91.40**	**88.30**	**94.40**	**85.40**	**99.30**	**–**	**88.08**	Overall accuracy (%)	**92.26**
	Level 2 (vegetated)	Bay tree	Oak tree	Shrub	Grass	Sum	User's %					Average accuracy (%)	**80.15**
	Bay tree	3030	895	49	14	3988	75.97					Overall accuracy (%)	**81.02**
	Oak tree	722	5525	140	0	6388	86.50					Kappa	**0.72456**
	Shrub	97	730	682	176	1685	40.49					Standard Deviation	**0.00453**
	Grass	35	7	94	3392	3528	96.15						
	Sum	3884	7157	965	3582	15588	–						
	Producer's %	**78.00**	**77.20**	**70.70**	**94.70**	**–**	**81.02**						
	Level 2 (non-vegetated)					Dead tree	Dry area	Wet area	Water	Sum	User's %	Average accuracy (%)	**94.10**
				Dead tree		4164	531	1761	0	6456	64.49	Overall accuracy (%)	**92.95**
				Dry area		77	11690	0	58	11825	98.85	Kappa	**0.90332**
				Wet area		56	0	10469	0	10525	99.47	Standard Deviation	**0.00180**
				Water		0	136	0	8236	8372	98.38		
				Sum		4297	12357	12230	8294	37178	–		
				Producer's %		**96.90**	**94.60**	**85.60**	**99.30**	**–**	**92.95**		
	Level 3							Non-stressed	Stressed	Sum	User's %	Average accuracy (%)	**75.55**
						Non-stressed		1422	517	1940	73.33	Overall accuracy (%)	**75.49**
						Stressed		397	1392	1788	77.82	Kappa	**0.51015**
						Sum		1819	1909	3728	–	Standard Deviation	**0.01049**
						Producer's		**78.20**	**72.90**	**–**	**75.49**		
	Final producer's accuracy for oak health levels:					Non-stressed		77.20(level 2) × 78.20(level 3) = **60.37**					
						Stressed		77.20(level 2) × 72.90(level 3) = **56.28**					

TABLE 3. SUMMARY OF OVERALL AVERAGE ACCURACY (OAA) OF CLASSIFICATION USING THE TWO FEATURE EXTRACTION METHODS

OAA (%)	Method 1 (Principal Components From Visible and NIR Bands)		Method 2 (Principal Components from All Bands)	
	Reflectance	Topographically Corrected Reflectance	Reflectance	Topographically Corrected Reflectance
Level 0 (eight classes)	89.82	88.08	89.49	86.93
Level 2 (four vegetated classes)	81.33	81.02	80.86	81.55
Level 2 (four non-vegetated classes)	95.09	92.95	94.78	90.81
Level 3 (two oak health classes)	74.06	75.49	74.44	74.84

TABLE 4. RESULTS OF *Z*-STATISTIC TEST CALCULATED FROM KAPPA-VARIANCE BETWEEN TWO DATA PREPROCESSING APPROACHES AND BETWEEN FEATURE EXTRACTION METHODS FOR SEPARATING THE TWO OAK HEALTH LEVELS: NON-STRESSED AND STRESSED

Test two data preprocessing approaches	Method 1 (PCA from visible and NIR bands)	Method 2 (PCA from all bands)
Reflectance versus topographically corrected reflectance	1.409	0.424
Test two feature extraction methods	Approach 1 (Reflectance)	Approach 2 (Topographically corrected reflectance)
Method 1 versus method 2	0.628	0.370

health levels (stressed and non-stressed) may be lower than 75 percent (or 60 percent and 56 percent for the joint accuracies). However, this result is still encouraging, especially considering the subtle spectral difference between the two levels of oak health and our previous work (Pu *et al.*, 2003b; Kelly and Liu, 2004).

There have been many studies on forest moisture stress detection and mapping with multi/hyperspectral remote sensing data, including both airborne and satellite remote sensing (e.g., Riggs and Running, 1991; Macomber and Woodcock, 1994). Water stress may be attributed to drought, diseases or both. Generally, this type of research suggests that canopy moisture stress would be detectable with remote sensing techniques only when it reaches a relatively high level. For example, Riggs and Running (1991) used Airborne Imaging Spectrometer (AIS-2) data to detect canopy water stress in conifers. They concluded that water stress in conifer canopies may not be routinely detectable at an operational landscape scale because they could not find any significant differences in reflectance between most coniferous stressed and controlled canopies. This lack of difference can be attributed to relatively low level of water stress, as well as high levels of variability in canopy conditions. This might play a particularly important role in hardwood canopies, where canopy condition is highly variable. In monitoring forest health conditions, especially hardwood oak forest diseases, airborne digital imageries have been successfully used to delineate or map dead and dying oak trees to monitor SOD in California (Kelly, 2002) and to detect oak wilt disease (Everitt *et al.*, 1999) in south-central Texas. Previous work (e.g., Riggs and Running, 1991; Everitt *et al.*, 1999) has demonstrated that detecting canopy moisture stress with airborne or satellite remote sensing imagery is only possible when the stress is very high. Forest health conditions can be monitored or mapped only for those severely infected (or affected) and dead or dying trees; this requires appropriate timing of imagery acquisition. We are encouraged by our experimental results derived from a multilevel classification scheme and hyperspectral remote sensing data; and anticipate that future efforts may be able to monitor and map forest moisture stress and other health conditions at earlier stages of stress, given sufficient attention is paid to spectral resolution, and timing of imagery acquisition.

Summary and Conclusions

In this study, a Compact Airborne Spectrographic Imager-2 (CASI) dataset was used for detecting mortality and vegetation stress associated with a new forest disease, sudden oak death (SOD). We first developed a multilevel classification scheme to increase classification accuracy of final classes. We next transformed the CASI radiance values to reflectance and corrected for topography and used a PCA transformation of all 48 CASI bands and the visible bands and NIR bands separately to extract features from CASI data. Finally, we classified each of the four datasets (created with the two data preprocessing approaches each with the two feature extraction methods) using a maximum likelihood classifier and tested the relative accuracies of each across the classification scheme. The multilevel scheme consists of four levels: Levels 0 through 3. Level 0 (a traditional classification scheme) was for the entire study area and classified eight classes found in the study area (California bay trees, oak trees, shrub areas, grasses, dead trees, dry areas, wet areas, and water). At Level 1, the vegetated and non-vegetated areas were separated using an NDVI threshold of 0.3 (all pixels greater than 0.3 assigned as vegetation). The vegetated and non-vegetated areas were further subdivided into four vegetated (bay trees, oak trees, shrub area, and grasses) and four non-vegetated (dead trees, dry and wet areas, and water body) classes at Level 2. Level 3 identified stressed and non-stressed oak trees.

According to the classification scheme, the more detailed classification level resulted in higher classification accuracy. When the CASI topographically corrected reflectance data were processed into ten PCs (five PCs from the visible region and five PCs from NIR bands) the classification accuracy (AA) for Level 2 vegetated classes increased to 80.15 percent from the classification accuracy at Level 0 (78.07 percent). The classification accuracy for Level 2 non-vegetated classes also increased to 94.10 percent from the classification accuracy at Level 0 (92.66 percent). Finally, we went from being unable to discriminate stressed and non-stressed oak trees at Level 0 to a classification accuracy of 75.55 percent (OAA = 75.49 percent) at Level 3. Particularly, it is encouraging that the two health levels of oak trees could be differentiated at a high classification level in spite of a relatively low classification accuracy in other classes. This is due to an increased spectral separability at the more detailed classification levels (Levels 2 and 3). Furthermore, the experimental results indicated that the feature extraction method using PCs from visible and NIR bands separately is better than those PCs from all 48 bands, especially for differentiating the two oak health levels at Level 3.

Acknowledgments

This research was partially funded by the NASA New Investigator Program to M. Kelly and the NASA EO-1 Science Validation Grant NCC5-492. Additional support came from the California Department of Forestry and Fire Protection. The CASI imagery was provided by USDA. We would like to thank David Shaari, Shaokui Ge, Yong Tian, Qian Yu, and Desheng Liu for their help in field sampling and spectral measurement. We also thank Faith Kearns for manuscript editing. This work was performed at U.C. Berkeley's Center for Assessment and Monitoring of Forest and Environmental Resources.

References

Allen, T.R., 2000. Topographic normalization of Landsat Thematic Mapper data in three mountain environments, *Geocarto International*, 15(2):13–19.

Belanger, M.J., J.R. Miller, and M.G. Boyer, 1995. Comparative relationships between some red edge parameters and seasonal leaf chlorophyll concentrations, *Canadian Journal of Remote Sensing*, 21(1):16–21.

Ceccato, P., S. Flasse, S. Tarantola, S. Jacquemoud, and J.-M. Gregoire, 2001. Detecting vegetation leaf water content using reflectance in the optical domain, *Remote Sensing of Environment*, 77(1):22–33.

Cibula, W.G., E.F. Zetka, and D.L. Rickman, 1992. Response of Thematic Mapper bands to plant water stress, *International Journal of Remote Sensing*, 13(10):1869–1880.

Collins, J.B., and C.E. Woodcock, 1996. An assessment of several linear change detection techniques for mapping forest mortality using multitemporal Landsat TM data, *Remote Sensing of Environment*, 56:66–77.

Congalton, R., and R.A. Mead, 1983. A quantitative method for consistency and correctness in photointerpretation, *Photogrammetric Engineering & Remote Sensing*, 49(1):69–74.

Coops, N.C., M.L. Smith, M.E. Martin, and S.V. Ollinger, 2003. Prediction of eucalypt foliage nitrogen content from satellite-derived hyperspectral data, *IEEE Transactions on Geoscience and Remote Sensing*, 41(6):1338–1346.

Curran, P.J., 1989. Remote sensing of foliar chemistry, *Remote Sensing of Environment*, 30:271–278.

Curran, P.J., J.A. Kupiec, and G.M. Smith, 1997. Remote sensing the biochemical composition of a slash pine canopy, *IEEE Transactions on Geoscience and Remote Sensing*, 35(2):415–420.

Elvidge, C.D., 1990. Visible and near infrared reflectance characteristics of dry plant materials, *International Journal of Remote Sensing*, 11:1775–1795.

Everitt, J.H., D.E. Escobar, D.N. Appel, W.G. Riggs, and M.R. Davis, 1999. Using airborne digital imagery for detecting oak wilt disease, *Plant Disease*, 83:502–505.

Freemantle, J.R., R. Pu, and J.R. Miller, 1992. Calibration of imaging spectrometer data to reflectance using pseudo-invariant features, *Proceedings of the 14th Canadian Symposium on Remote Sensing*, Toronto, Ontario, 01–04, June, pp. 452–455.

Fung, T., and E. LeDrew, 1988. The determination of optimal threshold levels for change detection using various accuracy indices, *Photogrammetric Engineering & Remote Sensing*, 54(10):1449–1454.

Garbelotto, M., P. Svihra, and D.M. Rizzo, 2001. Sudden Oak Death syndrome fells three oak species, *California Agriculture*, 55:9–19.

Gerylo, G.R., R.J. Hall, S.E. Franklin, and L. Smith, 2002. Empirical relations between Landsat TM spectral response and forest stands near Fort Simpson, Northwest Territories, Canada, *Canadian Journal of Remote Sensing*, 28:68–79.

Goetz, A.F.H., J.W. Boardman, B. Kindel, and K.B. Heidebrecht, 1997. Atmospheric corrections: On deriving surface reflectance from hyperspectral images, *Proceedings of SPIE: Imaging Spectrometry III*, 3118:14–22.

Gong, P., 1993. Change detection using principal component analysis and fuzzy set theory, *Canadian Journal of Remote Sensing*, 19(1):22–29.

Gong, P., R. Pu, and B. Yu, 1997. Conifer species recognition: An exploratory analysis of in situ hyperspectral data, *Remote Sensing of Environment*, 62:189–200.

Gong, P., R. Pu, G.S. Biging, and M.R. Larrieu, 2003. Estimation of forest leaf area index using vegetation indices derived from Hyperion hyperspectral data, *IEEE Transactions on Geoscience and Remote Sensing*, 41(6):1355–1362.

Haboudane, D, J.R. Miller, N. Tremblay, P.J. Zarco-Tejada, and L. Dextraze, 2002. Integrated narrow-band vegetation indices for prediction of crop chlorophyll content for application to precision agriculture, *Remote Sensing of Environment*, 81(2–3):416–426.

Hall, R.J., S.E. Franklin, G.R. Gerylo, and A. Roberts, 1998. Estimation of crown closure and species composition from high resolution multispectral imagery, *Automated Interpretation of High Spatial Resolution Digital Imagery for Forestry* (D.A. Hill and D.G. Leckie, editors), Victoria, British Columbia, Canada, 10–12 February, pp. 309–320.

Hayer, D.J., and S.A. Sader, 2001. Comparison of change-detection techniques for monitoring tropical forest clearing and vegetation regrowth in a time series, *Photogrammetric Engineering & Remote Sensing*, 67(9):1067–1075.

Hsu, P.-H., Y.-H. Tseng, and P. Gong, 2002. Dimension reduction of hyperspectral images, *Geographic Information Sciences*, 8:1–8.

Imanishi, J, K. Sugimoto, and Y. Morimoto, 2004. Detecting drought status and LAI of two Quercus species canopies using derivative spectra, *Computers and Electronics In Agriculture*, 43(2):109–129.

Johnson, L.F., C.A. Hlavka, and D.L. Peterson, 1994. Multivariate analysis of AVIRIS data for canopy biochemical estimation along the Oregon transect, *Remote Sensing of Environment*, 47:216–230.

Kelly, M., D. Shaari, Q. Guo, and D. Liu, 2004. A comparison of standard and hybrid classifier methods for mapping hardwood mortality in areas affected by sudden oak death, *Photogrammetric Engineering & Remote Sensing*, 70(11):1229–123.

Kelly, N.M., and D. Liu, 2004. Mapping diseased oak trees using ADAR imagery, *Geocarto International*, 19(1):57–64.

Kelly, N.M., and R. Meentemeyer, 2002. Landscape dynamics of the spread of Sudden Oak Death, *Photogrammetric Engineering & Remote Sensing*, 68:1001–1009.

Kelly, N.M., 2002. Monitoring Sudden Oak Death in California using high-resolution imagery, *Proceedings of the Fifth Symposium on Oak Woodlands: Oak in California's Changing Landscape*, 23–25 October 2001, San Diego, California, USDA-Forest Service, General Technical Report PSW-GTR-184, Pacific Southwest Forest and Range Experimental Station, Berkeley, California, pp. 799–810.

Macomber, S., and C. Woodcock, 1994. Mapping and monitoring conifer mortality using remote sensing in the Lake Tahoe basin, *Remote Sensing of Environment*, 50:255–266.

Matson, P.A., L.F. Johnson, J.R. Miller, C.R. Billow, and R. Pu, 1994. Seasonal changes in canopy chemistry across the Oregon transect: Patterns and spectral measurement with remote sensing, *Ecological Applications*, 4:280–298.

McPherson, B.A., D.L. Wood, A.J. Storer, P. Svihra, D.M. Rizzo, N.M. Kelly, and R.B. Standiford, 2000. Oak mortality syndrome: Sudden death of oaks and tanoaks, *Tree Notes*, No. 26, pp. 1–6.

McPherson, B.A., D.L. Wood, P. Švihra, N.M. Kelly, A.J. Storer, and R.B. Standiford, 2005. Sudden oak death in California: Disease progression in oaks and tanoaks, *Journal of Forest Ecology and Management*, 213(1–3):71–89.

Meyer, P., K.I. Itten, T. Kellenberger, S. Sandmeier, and R. Sandmeier, 1993. Radiometric corrections of topographically induced effects on Landsat TM data in an alpine environment, *ISPRS Journal of Photogrammetry and Remote Sensing*, 48(4):17–28.

Peñuelas, J., I. Filella, and L. Sweeano, 1996. Cell wall elastivity and water index (R970nm/R900nm) in wheat under different nitrogen availabilities, *International Journal of Remote Sensing*, 17:373–382.

Peñuelas, J., I. Filella, C. Biel, L. Sweeano, and R. Save, 1993. The reflectance at the 950–970 nm region as an indicator of plant water status, *International Journal of Remote Sensing*, 14:1887–1905.

Pu, R., L. Foschi, and P. Gong, 2004. Spectral feature analysis for assessment of water status and health level of coast live oak (*Quercus agrifolia)* leaves, *International Journal of Remote Sensing*, 25(20):4267–4286.

Pu, R., P. Gong, G.S. Biging, and M.R. Larrieu, 2003a. Extraction of red edge optical parameters from Hyperion data for estimation of forest leaf area index, *IEEE Transactions on Geoscience and Remote Sensing*, 41(4):916–921.

Pu, R., S. Ge, N.M. Kelly, and P. Gong, 2003b. Spectral absorption features as indicators of water status in *Quercus agrifolia* leaves, *International Journal of Remote Sensing*, 24(9):1799–1810.

Richards, J.A., 1993. *Remote Sensing Digital Image Analysis*, Springer-Verlag, New York.

Riggs, G.A., and S.W. Running, 1991. Detection of canopy water stress in conifers using the Airborne Imaging Spectrometer, *Remote Sensing of Environment*, 35:51–68.

Rizzo, D.M., and M. Garbelotto, 2003. Sudden oak death: Endangering California and Oregon forest ecosystems, *Frontiers in Ecology and the Environment*, 1(5):197–204.

Rizzo, D.M., M. Garbelotto, J.M. Davidson, G.W. Slaughter, and S.T. Koike, 2002. *Phytophthora ramorum* as the cause of extensive mortality of *Quercus* spp. and *Lithocarpus densiflorus* in California, *Plant Disease*, 86:205–214.

Sampson, P.H., P.J. Zarco-Tejada, G.H. Mohammed, J.R. Miller, T.L. Noland, 2003. Hyperspectral remote sensing of forest condition: Estimating chlorophyll content in tolerant hardwoods, *Forest Science*, 49(3):381–391.

Smith, M.L., M.E. Martin, L. Plourde, and S.V. Ollinger, 2003. Analysis of hyperspectral data for estimation of temperate forest canopy nitrogen concentration: Comparison between an airborne (AVIRIS) and a spaceborne (Hyperion) sensor, *IEEE Transactions on Geoscience and Remote Sensing*, 41(6):1332–1337.

Tian, Q., Q. Tong, R. Pu, X. Guo, and C. Zhao, 2001. Spectroscopic determination of wheat water status using 1650–1850 nm spectral absorption features, *International Journal of Remote Sensing*, 22:2329–2338.

Townsend, P.A., and J.R. Foster, 2002. Terrain normalization of AVIRIS and Hyperion imagery in forested landscapes, *Proceedings of the Eleventh JPL Airborne Earth Science Workshop* (R.O. Green, editor), Pasadena, California, 05–08 March, pp. 1–5.

Townsend, P.A., and S.J. Walsh, 2001. Remote sensing of forested wetlands: Application of multitemporal and multispectral satellite imagery to determine plant community composition and structure in southeastern USA, *Plant Ecology*, 157:129–149.

Townsend, P.A., J.R. Foster, Jr. R.A. Chastain, and W.S. Currie, 2003. Application of imaging spectroscopy to mapping canopy nitrogen in the forests of the central Appalachian Mountains using Hyperion and AVIRIS, *IEEE Transactions on Geoscience and Remote Sensing*, 41(6):1347–1354.

Ustin, S.L., D.A. Roberts, J. Pinzón, S. Jacquemoud, M. Gardner, G. Scheer, C.M. Castañeda, and A. Palacios-Orueta, 1998. Estimating canopy water content of chaparral shrubs using optical methods, *Remote Sensing of Environment*, 65:280–291.

van Aardt, J.A.N, and R.H. Wynne, 2001. Spectral separability among six southern tree species, *Photogrammetric Engineering & Remote Sensing*, 67(12):1367–1375.

Wessman, C.A., J.D. Aber, and D.L. Peterson, 1989. An evaluation of imaging spectrometry for estimating forest canopy chemistry, *International Journal of Remote Sensing*, 10:1293–1316.

Wessman, C.A., J.D. Aber, D.L. Peterson, and J.M Melillo, 1988. Remote sensing of canopy chemistry and nitrogen cycling in temperate forest ecosystems, *Nature*, 335:154–156.

Yu, B., I.M. Osland, P. Gong, and R. Pu, 1999. Penalized discriminant analysis of *in situ* hyperspectral data for conifer species recognition, *IEEE Transactions on Geoscience and Remote Sensing*, 37:2569–2577.

(Received 06 January 2006; accepted 12 May 2006; revised 07 June 2006)